PAPER • OPEN ACCESS

Spin-wave excitations in presence of nanoclusters of magnetic impurities

To cite this article: Akash Chakraborty *et al* 2014 *New J. Phys.* **16** 033004

View the article online for updates and enhancements.

Spin-wave excitations in presence of nanoclusters of magnetic impurities

Akash Chakraborty[1,2,3]**, Paul Wenk**[3]**, Stefan Kettemann**[2,4]**, Richard Bouzerar**[5] **and Georges Bouzerar**[5]

[1] Institut für Theoretische Festkörperphysik, Karlsruhe Institute of Technology, D-76128 Karlsruhe, Germany
[2] School of Engineering and Science, Jacobs University Bremen, Campus Ring 1, D-28759 Bremen, Germany
[3] Institut I-Theoretische Physik, Universität Regensburg, D-93040 Regensburg, Germany
[4] Division of Advanced Materials Science, Pohang University of Science and Technology (POSTECH), Pohang 790-784, Korea
[5] Institut Néel, CNRS, Département MCBT, 25 avenue des Martyrs, B.P. 166, F-38042 Grenoble Cedex 09, France
E-mail: akash.chakraborty@physik.uni-regensburg.de

Abstract

Nanoscale inhomogeneities and impurity clustering are often found to drastically affect the magnetic and transport properties in disordered/diluted systems, giving rise to rich and complex phenomena. However, the physics of these systems still remains to be explored in more detail as can be seen from the scarce literature available. We present a detailed theoretical analysis of the effects of nanoscale inhomogeneities on the spin excitation spectrum in diluted magnetic systems. The calculations are performed on relatively large systems (up to $N = 66^3$). It is found that even low concentrations of inhomogeneities have drastic effects on both the magnon density of states and magnon excitations. These effects become even more pronounced in the case of short-ranged magnetic interactions between the impurities. In contrast to the increase of critical temperatures T_C, reported in previous studies, the spin-stiffness D is systematically suppressed in the presence of nanoscale inhomogeneities. Moreover D is found to strongly depend on the inhomogeneities' concentration, the cluster size, as well as the range of the

magnetic interactions. The findings are discussed in the prospect of potential spintronics applications. We believe that this detailed numerical work could initiate future experimental studies to probe this rich physics with the most appropriate tool, inelastic neutron scattering.

Keywords: spin-waves, nanoscale inhomogeneities, diluted magnetic systems, magnons, spin-stiffness

1. Introduction

Disordered magnetic systems, such as transition metal alloys [1–3], diluted magnetic semiconductors (DMSs) [4–6], diluted magnetic oxides [7, 8], and manganites [9–11] have continued to attract considerable attention ever since their respective discoveries. The prospects of these materials for novel spintronic devices led to a plethora of work from both the experimental as well as the theoretical point of view. For a long time the major focus of spintronics research was mostly on homogeneously diluted systems (with magnetic impurities distributed randomly on the host lattice), which were believed to give rise to the much coveted room-temperature ferromagnetism. For this purpose, huge efforts to grow systems as 'clean' as possible were made. However, in contrast to the common belief, this does not systematically appear to be the optimal route to room-temperature ferromagnetism. For instance, in homogeneously or well-annealed Mn-doped III-V DMSs it has been impossible, so far, to go beyond the critical temperature of 140 K for 5% Mn [12–14].

These findings led researchers to look into other possible avenues in the ultimate quest for the room-temperature phenomenon. Transmission electron microscopy (TEM) experiments revealed the presence of coherent Mn-rich spherical nanocrystals in (Ga, Mn)As [15, 16], which exhibited a Curie temperature of $\sim$360 K. A careful micro-structure analysis revealed the cluster structure to be coherent with that of the host matrix (zinc-blende type), and this ruled out the possibility of any inter-metallic precipitates or phase separation in these materials. Similar nanoscale clusters were also reportedly observed in other diluted materials like (Ge, Mn) [17–19] and (Zn, Co)O [20], exhibiting critical temperatures in excess of 300 K. A recent TEM-based study on (In,Fe)As [21] has also reported the presence of magnetic clusters, which were neither metallic Fe nor inter-metallic FeAs compounds. The nanoscale spinodal decomposition into regions with high and low concentration of magnetic ions was speculated to be the possible reason for the apparently high Curie temperatures in these compounds. Nanoscale inhomogeneities have also often been detected in other families of compounds. In manganites, inhomogeneities arise due to the interplay between the charge, spin, orbital, and lattice degrees of freedom, leading to the coexistence of metallic and insulating phases. For example, scanning tunneling spectroscopy images of $La_{1-x}Ca_xMnO_3$ revealed a clear phase separation just below the critical temperature [22]. It is widely believed that the phase separation is at the origin of the well known colossal magneto-resistance effect [23, 24]. In high T_C superconductors experimental studies often indicate the crucial role of inhomogeneities [25–27]. For example in [27], it was found that regions with weak superconductivity can persist to higher temperatures if bordered by regions of strong superconductivity. The possibility of increasing the maximum transition temperature by controlled distribution of the dopants has also been suggested.

Despite the existence of numerous experimental studies, the effects of nanoscale inhomogeneities in disordered and diluted systems still remain largely unexplored on the theoretical front. Because of the large supercells required, density functional theory-based calculations for inhomogeneous systems are considerably difficult. For the same reason the essentially exact Monte Carlo studies are unfortunately incapable to deal with these systems. Moreover the crucial importance of both thermal and transverse fluctuations calls for the inevitable need of an exact treatment of the disorder effects, which implies a real space treatment. Recently using a real-space RPA approach, able to handle considerably large system sizes, it has been demonstrated that nanoscale inhomogeneities can lead to a dramatic increase of the Curie temperatures [28]. The question which naturally arises is how impurity clustering affects the spin excitation spectrum? Indeed the spin-wave excitations provide valuable insight into the underlying spin dynamics of the system. Inelastic neutron scattering (INS) is a powerful experimental tool in this context, as the dispersion relation and the magnon damping can be measured directly and accurately. In contrast to non-dilute systems, such as manganites [29, 30], cobaltites [31, 32], multiferroics [33, 34], pnictides [35, 36] etc one can find very few detailed studies [37] devoted to spin dynamics in dilute magnetic systems. Note that until now no experimental data has been reported for spin excitations in III-V DMSs, such as (Ga, Mn)As.

2. Theoretical approach and the model

The aim of the current work is to provide such a detailed theoretical account of the spin excitation spectrum of diluted magnetic systems in the presence of nanoscale inhomogeneities. We show that nanoclusters of magnetic impurities can have drastic effects on the magnon density of states (DOS), the dynamical spectral function, as well as the spin-stiffness in these systems, when compared to the homogeneously diluted case. We recall that the homogeneous case refers to a random and uncorrelated distribution of the impurities without any nanoclusters. In our calculations, we have assumed for the lattice a simple cubic structure with periodic boundary conditions. In order to avoid additional parameters, the total concentration of impurities in the whole system is fixed to $x = 0.07$. The inhomogeneities are assumed to be spherical of radii r_0 and the concentration inside each of these nanospheres is denoted by x_{in}. For simplicity we also fix $x_{in} = 0.8$ for all cases considered in this study. This implies that for a size $r_0 = 2a$ (where a is the lattice spacing) each nanosphere contains 26 impurities for this x_{in}. We define the concentration of nanospheres in the system as $x_{ns} = N_S/N$, where N_S is the total number of sites included in all the nanospheres and $N = L^3$ is the total number of sites in the lattice. A variable $P_N = (x_{in}/x)x_{ns}$, is used to represent the total fraction of impurities contained within the nanospheres. For a particular disorder configuration the nanospheres are chosen in a random manner on the lattice, the only restriction imposed is to avoid any overlapping between them. The overlapping is avoided to ensure that we always have well-defined clusters, as the aim is to clearly identify the effects of a given kind of inhomogeneity on the magnetic properties. Nevertheless, even without this restriction we have checked that the effects are negligible on the results, and the conclusions in general are not affected. A schematic illustration of a typical disorder configuration and the methodology is given in figure 1. This model can be useful for a qualitative study of materials such as (Ga, Mn)As or (Zn, Co)O, where coherent spherical nanoclusters with diameters in the range of 5–50 nm were reported [15, 16, 20].
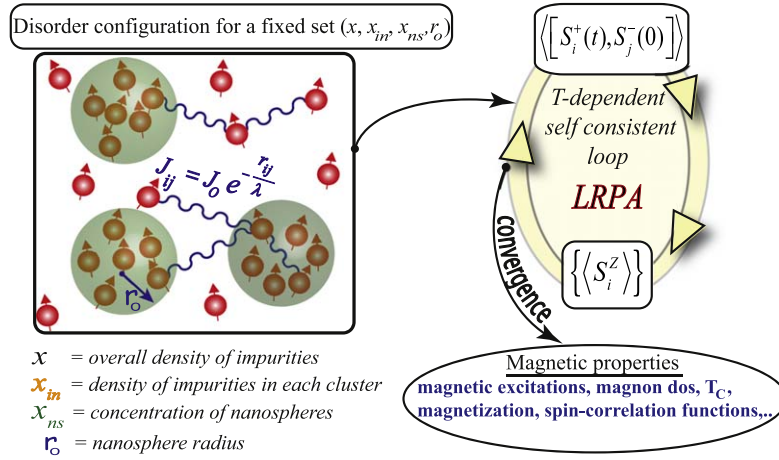
Figure 1. Schematic representation of a disorder configuration, illustrating the model parameters, and the self-consistent local RPA method.

We start with a Hamiltonian describing N_{imp} interacting spins randomly distributed on a lattice of N sites, which is given by the diluted random Heisenberg model

$$H_{Heis} = -\sum_{i,j} J_{ij} p_i p_j \mathbf{S}_i \cdot \mathbf{S}_j \tag{1}$$

where the sum ij runs over all sites and the random variable p_i is 1 if the site is occupied by an impurity, otherwise it is 0. The above Hamiltonian (1) is treated within the self-consistent local random phase approximation (SC-LRPA), which is a semi-analytical approach based on finite temperature Green's functions. Within this approach, the retarded Green's functions are defined as $G_{ij}^c(\omega) = \int_{-\infty}^{+\infty} G_{ij}^c(t) e^{i\omega t} dt$, where $G_{ij}^c(t) = -i\theta(t) \langle [\mathbf{S}_i^+(t), \mathbf{S}_j^-(0)] \rangle$, ($\langle \ldots \rangle$ denotes the thermal average). This describes the transverse spin fluctuations and the index 'c' denotes the disorder configuration. Note that the notation $G_{ij}^c(\omega)$ is equivalent to $G^c(r_i, r_j, \omega)$. After performing the Tyablicov decoupling of the higher-order Green's functions which appear in the equation of motion of $G_{ij}^c(\omega)$ one gets,

$$G_{ij}^c(\omega) = \sum_\alpha \frac{2\langle S_j^z \rangle}{\omega - \omega_\alpha^c + i\epsilon} \langle i \mid \Psi_\alpha^{R,c} \rangle \langle \Psi_\alpha^{L,c} \mid j \rangle \tag{2}$$

where $\langle S_j^z \rangle$ are the local magnetizations which have to be calculated self-consistently. $\left| \Psi_\alpha^{R,c} \right\rangle$ and $\left| \Psi_\alpha^{L,c} \right\rangle$ are respectively the right and left eigenvectors, associated with the same eigenvalue ω_α^c of the effective Hamiltonian $\mathbf{H}_{eff}^c$, whose matrix elements are given by

$$\left(\mathbf{H}_{eff}^c \right)_{ij} = -\langle S_i^z \rangle J_{ij} + \delta_{ij} \sum_l \langle S_l^z \rangle J_{lj} \tag{3}$$

where c denotes the configuration, i, j, l are the site indices, and z is the polarization direction. At finite temperature, $\mathbf{H}_{eff}^c$ is non-Hermitian (real and not necessarily symmetric) but it is bi-orthogonal [38]. The property of bi-orthogonality requires the calculation of the left and right eigenvectors, both associated with the same eigenvalue. However, since in the present case all calculations are performed at $T = 0$ K, the matrix $\mathbf{H}_{eff}^c$ is real symmetric, and the left and right

eigenvectors are identical. Also, since at $T = 0$ K the ground state is fully polarized, all $\langle S_i^z \rangle$'s $= S$ in this case. For more details on the SC-LRPA approach one can see for example [5, 39, 40]. The SC-LRPA was previously successfully implemented to calculate the magnetic excitation spectra in the nearest-neighbor diluted Heisenberg model [41] as well as in the case of optimally annealed (Ga, Mn)As [42]. In the latter case, an especially good agreement with experiments [43, 44] was also found.

Now it is well known from first principles based studies as well as model calculations that the exchange couplings in III-V DMS compounds are relatively short-ranged, non-oscillating, and almost exponentially decaying in nature [42, 45, 46]. This was the primary motivation to assume generalized couplings of the form $J_{ij} = J_0 \exp(-|\mathbf{r}_i - \mathbf{r}_j|/\lambda)$, where λ is the damping parameter. For this damping parameter, we focus here on two particular values, $\lambda = a$ and $a/2$ (a is the lattice spacing), corresponding to relatively long-ranged and short-ranged couplings respectively. It is worth noting that for about 5% Mn-doped GaAs, a fit of the *ab initio* exchange couplings leads to a value of λ of the order of $a/2$. Only recently it was shown that just varying λ within this scale can give rise to rather spectacular effects on the Curie temperatures in these inhomogeneous diluted systems [28]. Note that the nature of the magnetic couplings could also depend on the concentration of the clusters and/or the density of impurities inside. However, computing these couplings involves extensive calculations, systematic sampling over disorder, and especially diagonalizing very large matrices, which is beyond the scope of the present work. Our current goal is to provide a detailed analysis of the effects of nanoscale inhomogeneities, in the presence of these generalized interactions, on the dynamical properties of diluted systems, but the conclusions drawn are general.

3. Numerical results and discussion

We first start with the calculation of the magnon DOS for the homogeneously diluted case. The average magnon DOS is given by $\rho_{avg}(\omega) = \frac{1}{N_{imp}} \sum_i \langle \rho_i^c(\omega) \rangle_c$, where $\rho_i^c(\omega)$ is the local magnon DOS, which reads $\rho_i^c(\omega) = -\frac{1}{2\pi \langle S_i^z \rangle} \mathrm{Im}\, G_{ii}^c(\omega)$. In what follows $\langle \dots \rangle_c$ denotes the average over disorder configurations. Figure 2 shows ρ_{avg} as a function of the energy ω, for the two different values of λ mentioned above. The average over disorder is performed for a few hundred configurations (typically 200) in all the following calculations, although it was found that about 100 configurations are sufficient for the sampling and the results converge beyond that. ρ_{avg} is found to exhibit a regular Gaussian-like shape for the case of $\lambda = a$. The broad peak is located at $0.42W$ with a half-width of about $0.36W$ (W is the magnon excitation bandwidth). For longer ranged couplings, ρ_{avg} remains essentially similar to that of $\lambda = a$. On the other hand, for short-ranged couplings ($\lambda = a/2$), ρ_{avg} has a more irregular and richer structure. The peak in ρ_{avg} is now located at much lower energy, $0.06W$, and a clear long tail extending toward the high energies with multiple shoulders appears. These irregular features can be attributed to regions of impurities which are weakly connected to each other due to the short-range nature of the interactions. Effectively they behave as isolated regions which have their own eigenmodes, and these in turn contribute to the irregular shoulders appearing in the DOS. These shoulders become even more pronounced for shorter ranged interactions. In the case of $\lambda = a$ these shoulders are absent because of the longer range nature of the couplings. It is interesting to note
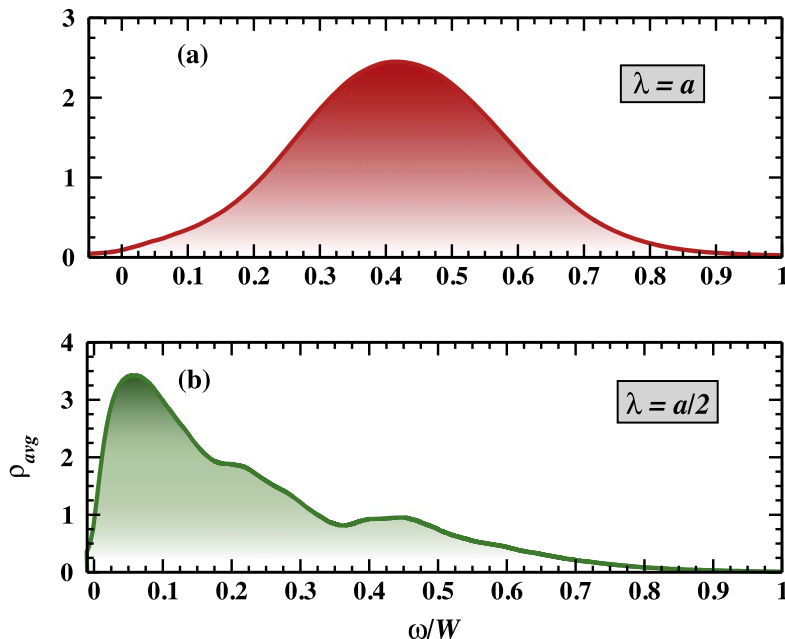
Figure 2. Average magnon DOS corresponding to the homogeneous case for (a) $\lambda = a$, and (b) $\lambda = a/2$. The average concentration is $x = 0.07$. The x-axis is in units of ω/W, where W is the magnon spectrum bandwidth. $W \approx 4J_0$ and $0.8J_0$, for $\lambda = a$ and $a/2$ respectively. The system size is $N = 56^3$.

that a similar kind of magnon DOS (as in figure 2(b)) was obtained in the case of (Ga, Mn)As [42]. However, in [42] the exchange couplings used had been directly calculated from the '*V-J*' model. It has been found that $\lambda = a/3$ provides a very good fit for these couplings.

In order to analyze the effects of inhomogeneities, we calculate in addition to ρ_{avg}, the local magnon DOS inside (ρ_{in}) and outside (ρ_{out}) the nanospheres. Unlike ρ_{avg}, the local DOS contains information on the nature of the magnon states, whether they are extended or localized. One can also calculate the typical DOS (which is essentially the geometric mean of the local DOS) which provide a direct access to the 'mobility edge' separating the localized modes from the extended ones. This can be the subject of a future detailed study. For the local DOS, we consider the particular case of nanospheres with fixed radii $r_0 = 2a$, concentration inside $x_{in} = 0.8$, and four different concentrations of nanospheres x_{ns}. The results for $\lambda = a$ are depicted in figure 3. Let us first focus on ρ_{avg}. From figure 3(a), we immediately notice that a relatively small concentration of inhomogeneities ($x_{ns} \sim 0.02$) causes a significant change in the magnon DOS. Indeed, in comparison to the homogeneous case, the excitations spectrum bandwidth is now doubled, and ρ_{avg} has a bimodal structure, with a broader peak at higher energies. With increasing x_{ns}, we observe a gradual transfer of weight from the low to high energy peak. The low energy peak shifts to smaller energies which is consistent with the decrease in the concentration of impurities outside the nanospheres. In order to have a better understanding of the features seen in ρ_{avg}, we now analyze ρ_{in} and ρ_{out}. We observe that ρ_{in} remains unchanged in all cases and exhibit a very small weight from 0 to $0.7W$. Thus the high energy peak seen in ρ_{avg} can clearly be attributed to the nanocluster modes. A careful analysis of
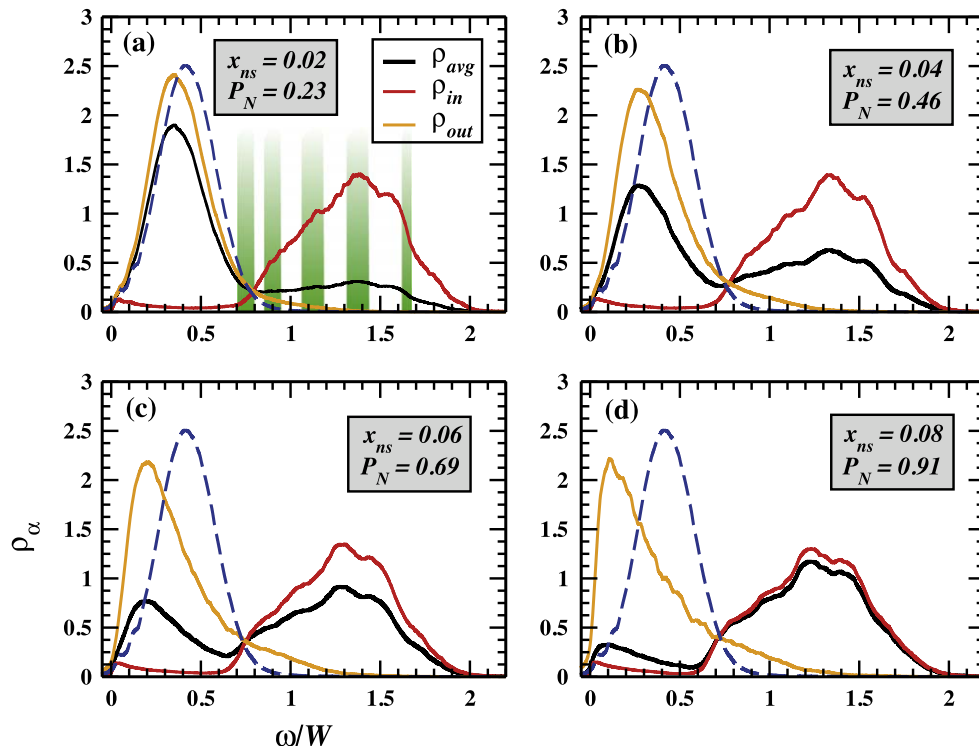
Figure 3. ρ_α denotes the average magnon DOS (ρ_{avg}), local magnon DOS inside (ρ_{in}), and outside the nanospheres (ρ_{out}), for four different x_{ns}. P_N is the percentage of total impurities inside the nanospheres. The blue dashed curves represent the homogeneous ρ_{avg} from figure 2(a). The shaded regions in (a) correspond to the calculated eigenmodes of a single isolated nanosphere. The parameters are $\lambda = a$, $r_0 = 2a$, and $x_{in} = 0.8$. The x-axis is in units of ω/W, where $W \approx 4J_0$ is homogeneous magnon bandwidth.

a single isolated cluster reveals that the first non-zero eigenmodes are located at $0.7W$, which explains the very small weight in ρ_{in} below this value. Note that in figure 3(a),the shaded regions correspond to the discrete spectrum of an isolated single nanosphere, which is calculated over a few hundred configurations (random position of the impurities inside the nanosphere). The weak variation of ρ_{in} with respect to x_{ns}, indicates that the disappearance of the discreteness in ρ_{in} (as seen in the isolated nanosphere spectrum) results mainly from the interactions between the cluster impurities and those outside. The above discussion of ρ_{avg} and ρ_{in} explains naturally the behavior of ρ_{out}. In the case of more extended couplings, it is expected that (i) ρ_{avg} loses progressively the bimodal nature, (ii) the pseudo-gap in ρ_{in} at low energies is filled gradually, and (iii) the second peak in ρ_{in} becomes narrower and shifts to higher energies with respect to the spectrum of a single isolated cluster.

We now discuss the effects of short-ranged interactions ($\lambda = a/2$) on the average and local magnon DOS. The results are shown in figure 4. The magnon bandwidth increases by 250% with respect to that of the homogeneous system. As seen before, we observe a clear transfer of weight in ρ_{avg}, from the low to the higher energies with increasing x_{ns}. In contrast to the bimodal nature observed for $\lambda = a$, ρ_{avg} now exhibits a long wavy tail, extending toward higher energies.
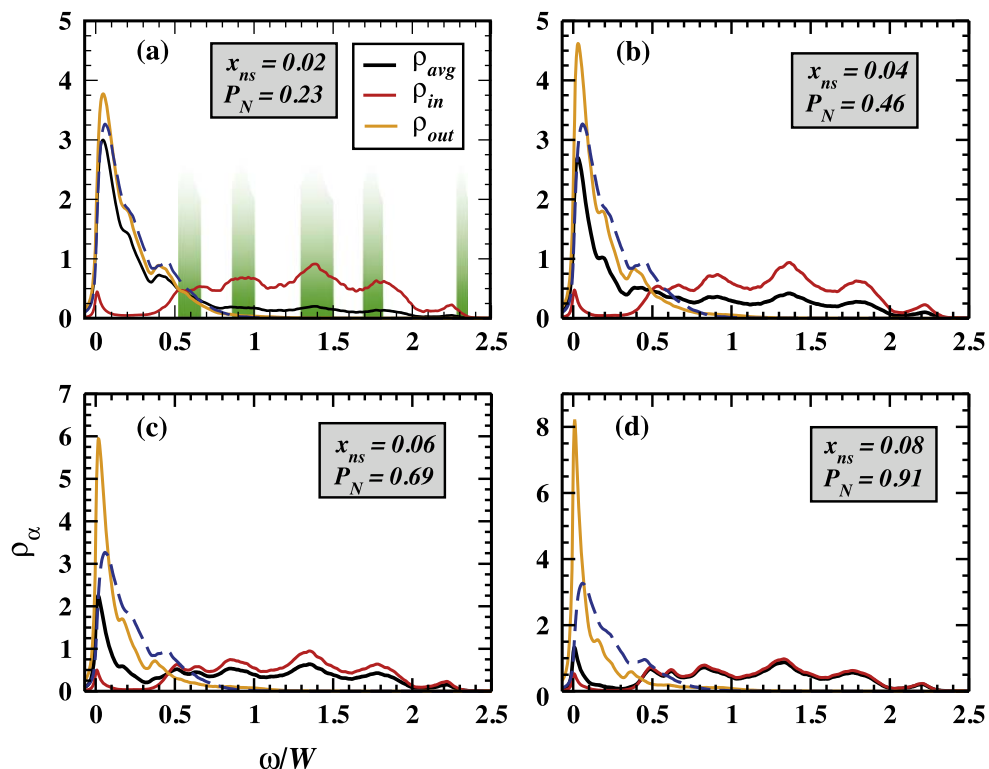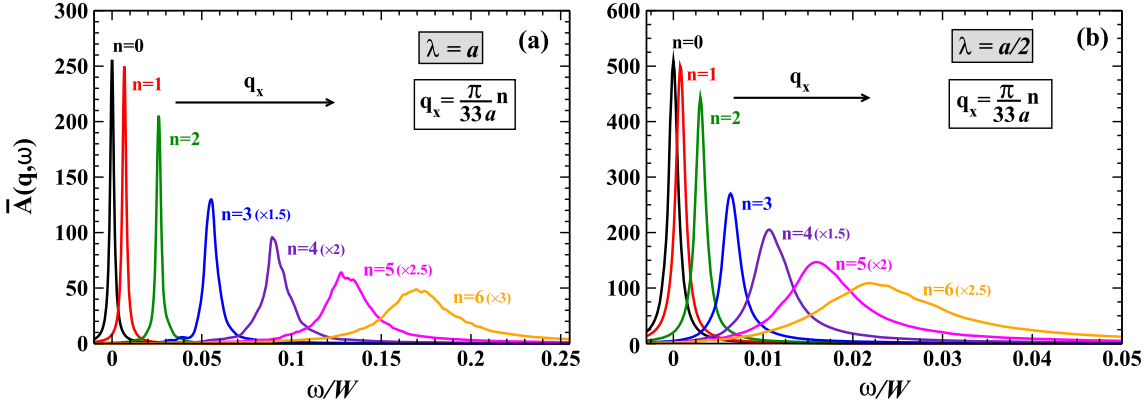
Figure 4. ρ_{avg}, ρ_{in}, and ρ_{out} for $\lambda = a/2$, for four different x_{ns}. The blue dashed curves represent the homogeneous ρ_{avg} from figure 2(b). The shaded regions in (a) correspond to the calculated eigenmodes of a single isolated nanosphere. The other parameters being same as in figure 3. The homogeneous magnon bandwidth is $W \approx 0.8 J_0$.

This wavy tail is actually attributed to the cluster impurities and is related to the nature of ρ_{in}, which is discussed in the following. ρ_{in} shows (i) a clear multiple peak structure now, (ii) is independent of x_{ns}, and (iii) a well-defined gap of approximately $0.5W$ is observed. The reasons for the appearance of these multiple peaks in ρ_{in} are the enhanced discreteness (larger sub-gaps) of the eigenmodes of the single isolated nanosphere and the reduced interactions of the cluster impurities with those outside. Concerning ρ_{out}, besides a shift to lower energies as seen for $\lambda = a$, we now observe that the peak becomes narrower with increase in x_{ns}. (The latter feature was absent for the long ranged couplings.) The reason for this is with increasing x_{ns}, the concentration of impurities outside decreases and the effective interactions between them become weaker. This effect will be even more pronounced for shorter ranged couplings. Even though the couplings are comparable, drastic changes between figures 3 and 4, shows that $\lambda = a$ corresponds to the intermediate range couplings and $\lambda = a/2$ definitely to the short-range regime.

We propose now to focus on the low energy excitation spectrum in these systems. For this purpose we evaluate the dynamical spectral function, which provides deeper insight into the underlying spin dynamics. This physical quantity can be directly and accurately probed by INS experiments. It is defined by $\bar{A}(\mathbf{q}, \omega) \equiv \langle A^c(\mathbf{q}, \omega) \rangle_c = - \left\langle \frac{1}{2\pi \langle \langle S^z \rangle \rangle} \text{Im } G^c(\mathbf{q}, \omega) \right\rangle_c$, where

Figure 5. Average spectral function $\bar{A}(\mathbf{q}, \omega)$ as a function of the energy in the [1 0 0] direction for different values of q_x, corresponding to the homogeneous case for (a) $\lambda = a$, and (b) $\lambda = a/2$. The energy axis (x-axis) is in units of ω/W. The system size is $N = 66^3$. (The intensity of the peaks have been multiplied by the factors indicated in the parentheses.)

$\langle\langle S^z \rangle\rangle = \frac{1}{N_{imp}}\sum_i \langle S_i^z \rangle$ is the total average magnetization over all spin sites, and $G^c(\mathbf{q}, \omega)$ is the Fourier transform of $G_{ij}^c(\omega)$ given in equation (2). The averaged dynamical spectral function is evaluated from the following

$$\bar{A}(\mathbf{q}, \omega) = \left\langle \sum_\alpha A_\alpha^c(\mathbf{q})\delta(\omega - \omega_\alpha^c) \right\rangle_c \tag{4}$$

where

$$A_\alpha^c(\mathbf{q}) = \frac{1}{N_{imp}}\sum_{ij}\lambda_j \langle i \mid \Psi_\alpha^{R,c} \rangle \langle \Psi_\alpha^{L,c} \mid j \rangle e^{i\mathbf{q}(\mathbf{r}_i - \mathbf{r}_j)} \tag{5}$$

where $\lambda_j = \frac{\langle S_j^z \rangle}{\langle\langle S^z \rangle\rangle}$ is the temperature dependent local parameter. Note that at $T = 0$ K, all λ_js = 1.

First we discuss the average spectral function for the homogeneously diluted systems. Figures 5(a) and (b) show $\bar{A}(\mathbf{q}, \omega)$, for $\lambda = a$ and $a/2$ respectively, as a function of the energy for different values of the momentum $\mathbf{q}$ in the [1 0 0] direction. First in both cases, as $\mathbf{q}$ increases the peaks become broader and more asymmetric with a tail extending toward higher energies. Well-defined excitations exist only for relatively small values of the momentum, beyond $q_x a \approx 0.24\pi$ ($n = 8$) no well-defined magnons exist. The increase in asymmetry with increasing $\mathbf{q}$ (i.e. shorter wavelength) is due to the decay of the collective spin-waves into localized excitations. A considerable softening of the spin-waves will be observed on approaching the Brillouin zone boundary, which is due to the localized nature of the high-energy magnon modes in this region. However, for $\lambda = a$, the well-defined excitations persist up to energy values of about $0.25W$, whilst for $\lambda = a/2$ the excitations reach only up to $0.035W$, where W is the λ-dependent magnon spectrum bandwidth. This difference in the range of energies, by one order of magnitude, can be attributed to the decrease in the range of the effective interactions. This also demonstrates, once again, the profound effects observed on going from $\lambda = a$ to $a/2$. We remind that $W \approx 4J_0$ and $0.8J_0$, for $\lambda = a$ and $a/2$, respectively.
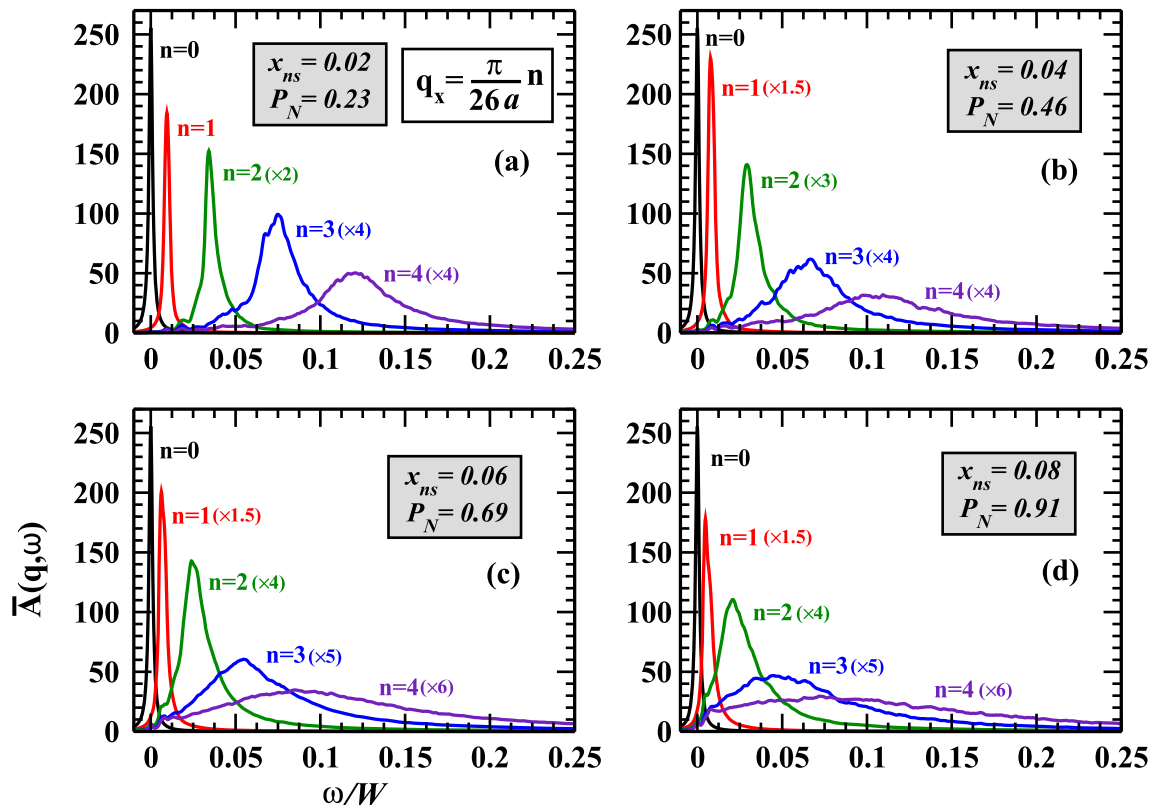
Figure 6. Average spectral function $\bar{A}(\mathbf{q}, \omega)$ as a function of the energy in the [1 0 0] direction, for four different x_{ns}. P_N indicates the percentage of total impurities inside the nanospheres. The parameters are $\lambda = a$, $r_0 = 2a$, $x_{in} = 0.8$, and $N = 52^3$. The x-axis is in units of ω/W. (The intensity of the peaks have been multiplied by the factors indicated in the parentheses.)

   We now proceed further and analyze the effects of nanoscale inhomogeneities on the dynamical spectral function. The results for $\lambda = a$ are depicted in figure 6. As we increase x_{ns}, there is a broadening in the excitations, accompanied with an increase in asymmetry and a shift toward the lower energies is observed. These effects are already pronounced even for the lowest concentration of nanospheres. For instance, for $q_x a \approx 0.12\pi$ ($n = 3$), the magnon energies are $0.09W$, $0.075W$, and $0.067W$, for $x_{ns} = 0$, 0.02, and 0.04, respectively. In order to analyze the effects of inhomogeneities on the magnon lifetime for a given $\mathbf{q}$, we define the ratio $R(\mathbf{q}) = \gamma(\mathbf{q})/\omega(\mathbf{q})$, where $\gamma(\mathbf{q})$ is the half-width of the excitations. The excitations are well-defined in character only when $R(\mathbf{q}) < 1$. For the aforesaid q_x, the corresponding $R(\mathbf{q})$s are 0.2, 0.33, and 0.66, for $x_{ns} = 0$, 0.02, and 0.04, which corresponds to an increase of about 60% and 200% respectively, compared to the homogeneous case, for these two values of x_{ns}. It is interesting to note that these effects could hardly be anticipated from the magnon DOS results (figure 3). In fact the analyses of the DOS suggested that the low energy excitations should be weakly affected by the inhomogeneities. In the following, we discuss the spectral function in the presence of short-ranged interactions, shown in figure 7. As in the previous case, well-defined excitations exist only for small values of the momentum. However, here we find that the shift toward the lower energies is strongly enhanced. If we consider the particular case of
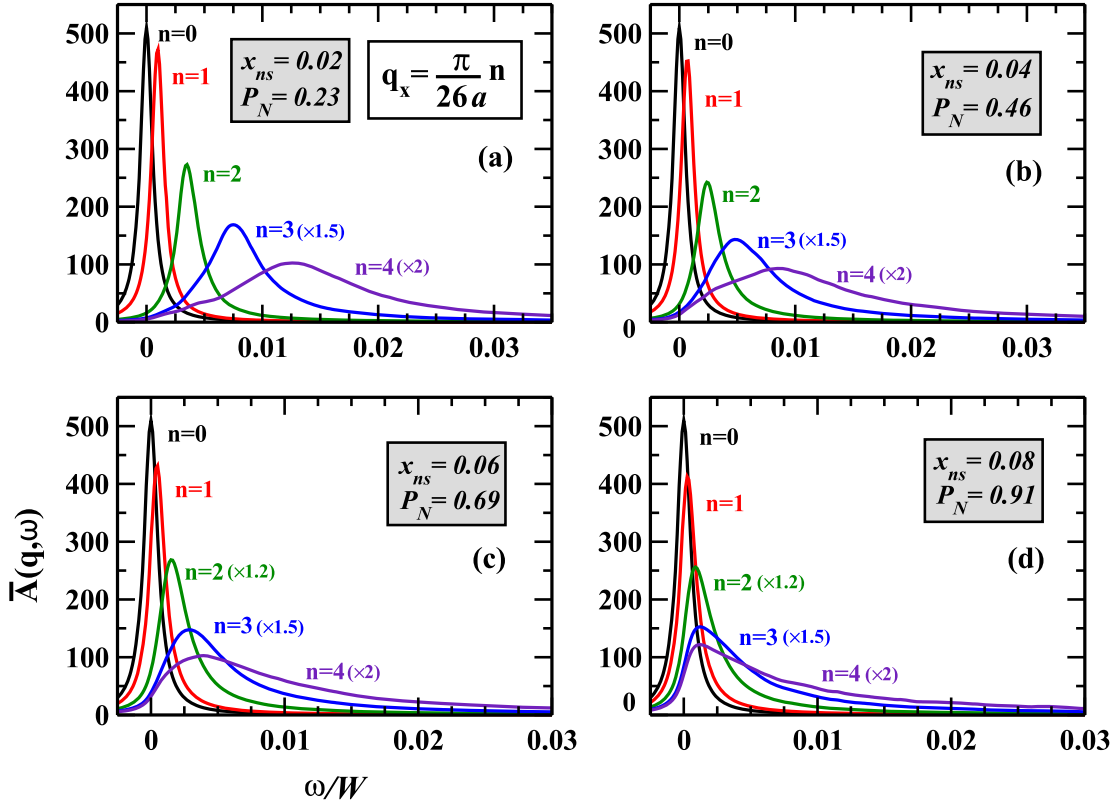
Figure 7. Average spectral function $\bar{A}(\mathbf{q}, \omega)$ for the case of $\lambda = a/2$, with the other parameters same as in figure 6.

$q_x a \approx 0.12\pi$, the magnon energies are shifted by 30% and 60% respectively, for $x_{ns} = 0.02$ and 0.04, with respect to that of the homogeneous case. The $R(\mathbf{q})$s for this value of q_x are 0.4, 0.8, and 1.3 for $x_{ns} = 0$, 0.02, and 0.04. This indicates that the excitations have dramatically lost their well-defined character as compared to the previous case (figure 6).

From the $\bar{A}(\mathbf{q}, \omega)$ calculations, we extract both the magnon dispersion $\omega(\mathbf{q})$ and the spin-stiffness D^{inh}. We remind that in the long wavelength limit, $\omega(\mathbf{q}) = D^{inh}q^2$. In order to gauge the effects of the inhomogeneities, we define the normalized spin-stiffness coefficient $D_n = D^{inh}/D^{hom}$, where D^{inh} denotes the spin-stiffness of the inhomogeneous systems, and D^{hom} that of the homogeneously diluted system. The values of D^{hom} are found to be 2.9 J_0 and 0.07 J_0, for $\lambda = a$ and $a/2$ respectively, for $x = 0.07$. We would like to stress that both $\omega(\mathbf{q})$ and D^{inh} were obtained from the first non-zero $\mathbf{q}$ excitations $\left(\mathbf{q} = \left(\frac{2\pi}{La}, 0, 0\right)\right)$ corresponding to system sizes $N = L^3$, where L varies from 36 to 52. Figures 8(a) and (b) show $\omega(\mathbf{q})$ as a function of $\mathbf{q}$ for various x_{ns}, corresponding to $\lambda = a$, and $a/2$ respectively. First, in both cases, we observe that the inhomogeneities suppress the magnon dispersion. This suppression is even more drastic in the case of short-ranged interactions. In addition, the quadratic behavior persists up to large $\mathbf{q}$ for $\lambda = a/2$, whilst a clear softening of the magnon modes can be seen in the case of the extended couplings, for $q_x/\pi \gtrsim 0.2$. This is consistent with the discussions of figures 6 and 7. The well-defined magnon region shrinks significantly on going from $\lambda = a$ to $\lambda = a/2$.
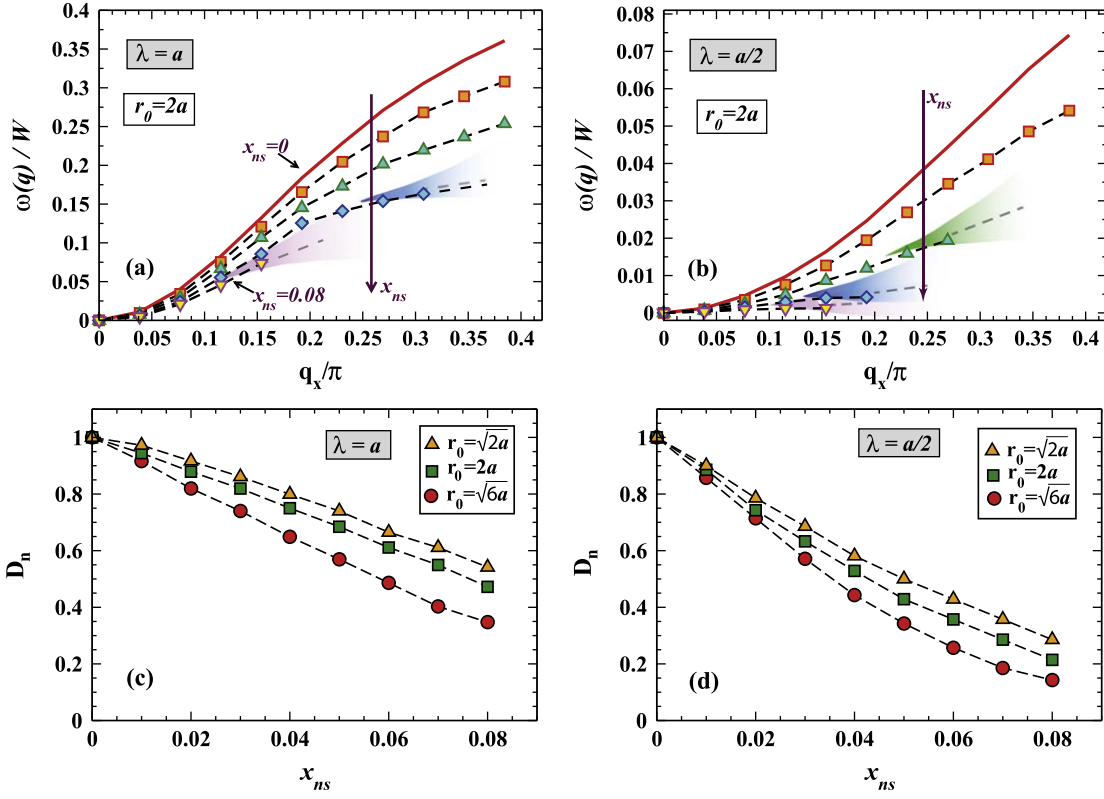
Figure 8. Magnon dispersion as a function of q_x/π, for different x_{ns} (0, 0.02, 0.04, 0.06, and 0.08) for (a) $\lambda = a$, and (b) $\lambda = a/2$. The vertical arrows indicate the direction of increasing x_{ns}. The solid (red) curve corresponds to the homogeneous case. The shaded regions indicate the q values beyond which there is no well-defined excitation. (c) and (d) show the normalized spin-stiffness D_n as a function of x_{ns}, corresponding to $\lambda = a$, and $\lambda = a/2$, respectively, for three different r_0: $\sqrt{6}\,a$, $2a$, and $\sqrt{2}\,a$. The concentration inside nanospheres is $x_{in} = 0.8$.

This tendency is enhanced on increasing x_{ns}. With increase in x_{ns}, the concentration of impurities outside the clusters gradually decreases since the overall concentration is fixed. Consequently the typical distance between the impurities outside increases and they are weakly coupled to the rest of the system. This leads to the suppression of the magnon modes with increasing x_{ns} and the effects are naturally more pronounced in the case of short-ranged interactions. In order to evaluate more quantitatively the effects of the inhomogeneities, the normalized spin-stiffness D_n is plotted in figures 8(c) and (d), as a function of x_{ns}, for various radii of the nanospheres. As anticipated from the previous figures, one observes for both $\lambda = a$ and $a/2$, a monotonous decrease of the spin-stiffness with increasing x_{ns}. D_n decreases almost linearly up to $x_{ns} \approx 0.04$, and the slope for $\lambda = a/2$ is twice that of $\lambda = a$. We find that the suppression of the spin-stiffness is greater for larger radii of the nanospheres. For instance, for the particular $x_{ns}=0.03$, the spin-stiffness is reduced by 15% for $r_0 = \sqrt{2}\,a$, and by almost 30% for $r_0 = \sqrt{6}\,a$, for $\lambda = a$ (figure 8(c)), although the concentration outside the nanospheres is almost the same. In the case of the short-ranged couplings this effect is even stronger. The effects of the nanoscale

inhomogeneities on the spin-stiffness are in striking contrast to that observed on the critical temperatures, where an increase by more than one order of magnitude was found [28].

4. Conclusion

To conclude, in this work we have shed light on the effects of nanoscale inhomogeneities on the magnetic excitation spectrum of dilute systems. To our knowledge, no such detailed numerical study has been performed so far. Compared to homogeneously diluted systems, even low concentrations of nanoscale inhomogeneities is sufficient to induce drastic changes in the magnon DOS. The magnon dispersion is found to vary significantly with the concentration of inhomogeneities, leading to a strong suppression of the spin-stiffness. This suppression of the dispersion can be ascribed to the reduction of the effective interactions with increase in the density of nanoclusters in the system. In the rapidly growing field of spintronics, most data storage devices use the dynamical motion of spins. In this context, this study on the spin-wave damping can be of practical interest. We also find a strong increase of the half-width of the magnon excitations in the long wavelength limit. These features are strongly enhanced in the case of short-ranged couplings. The lifetime of the excitations (which is inversely proportional to the half-width) is also relevant from the applications aspect. A short lifetime is essential for memory devices, to leave a bit in a steady state after a read-in or read-out operation. A longer lifetime, on the other hand, is necessary for the unhampered transmission of signals in inter-chip communications. It would also be interesting to study the effects of temperature on the spin dynamics of these inhomogeneous systems. We expect the temperature dependence of the spin-stiffness, especially in systems with short-ranged interactions, to be unconventional compared to that of the homogeneous systems. Another follow up to this work would be to calculate the couplings, within a non-perturbative approach, in the presence of the inhomogeneities. The present findings already provide qualitative insights and these could be useful in understanding further calculations. Finally, we believe this detailed study would serve to motivate future experimental works on these inhomogeneous compounds.

Acknowledgments

References

[1] Moruzzi V L 1990 *Phys. Rev.* B **41** 6939
[2] Abrikosov I A, Eriksson O, Söderlind P, Skriver H L and Johansson B 1995 *Phys. Rev.* B **51** 1058
[3] James P, Eriksson O, Johansson B and Abrikosov I A 1999 *Phys. Rev.* B **59** 419
[4] Jungwirth T, Sinova J, Masek J, Kucera J and MacDonald A H 2006 *Rev. Mod. Phys.* **78** 809
[5] Sato K *et al* 2010 *Rev. Mod. Phys.* **82** 1633
[6] Timm C 2003 *J. Phys. Condens. Matter* **15** R1865
[7] Fukumura T, Toyosaki H and Yamada Y 2005 *Semicond. Sci. Technol.* **20** S103

[8] Chambers S A, Droubay T C, Wang C M, Rosso K M, Heald S M, Schwartz D A, Kittilstved K R and Gamelin D R 2006 *Mater. Today* **9** 28

[9] Salamon M B and Jaime M 2001 *Rev. Mod. Phys.* **73** 583

[10] Goto T, Kimura T, Lawes G, Ramirez A P and Tokura Y 2004 *Phys. Rev. Lett.* **92** 257201

[11] Dagotto E 2002 *Nanoscale Phase Separation and Colossal Magnetoresistance* (Berlin: Springer)

[12] Edmonds K W, Wang K Y, Campion R P, Neumann A C, Farley N R S, Gallagher B L and Foxon C T 2002 *Appl. Phys. Lett.* **81** 4991

[13] Ku K C *et al* 2003 *Appl. Phys. Lett.* **82** 2302

[14] Bouzerar R and Bouzerar G 2010 *Europhys. Lett.* **92** 47006

[15] Moreno M, Trampert A, Jenichen B, Däweritz L and Ploog K H 2002 *J. Appl. Phys.* **92** 4672

[16] Yokoyama M, Yamaguchi H, Ogawa T and Tanaka M 2005 *J. Appl. Phys.* **97** 10D317

[17] Xiu F, Wang Y, Kim J, Hong A, Tang J, Jacob A P, Zou J and Wang K L 2010 *Nat. Mater.* **9** 337

[18] Bougeard D, Ahlers S, Trampert A, Sircar N and Abstreiter G 2006 *Phys. Rev. Lett.* **97** 237202

[19] Park Y D, Wilson A, Hanbicki A T, Mattson J E, Ambrose T, Spanos G and Jonker B T 2001 *Appl. Phys. Lett.* **78** 2739

[20] Jedrecy N, von Bardeleben H J and Demaille D 2009 *Phys. Rev. B* **80** 205204

[21] Tanaka M, Ohya S and Hai P N 2014 *Appl. Phys. Rev.* **1** 011102

[22] Fäth M, Freisem S, Menovsky A A, Tomioka Y, Aarts J and Mydosh J A 1999 *Science* **285** 1540

[23] von Helmholt R, Wecker J, Holzapfel B, Schultz L and Samwer K 1993 *Phys. Rev. Lett.* **71** 2331

[24] Jin S, Tiefel T H, McCormack M, Fastnacht R A, Ramesh R and Chen L H 1994 *Science* **264** 413

[25] Pan S H *et al* 2001 *Nature* **413** 282

[26] Wise W D *et al* 2009 *Nat. Phys.* **5** 213

[27] Parker C V, Pushp A, Pasupathy A N, Gomes K J, Wen J, Xu Z, Ono S, Gu G and Yazdani A 2010 *Phys. Rev. Lett.* **104** 117001

[28] Chakraborty A, Bouzerar R, Kettemann S and Bouzerar G 2012 *Phys. Rev. B* **85** 014201

[29] Motome Y and Furukawa N 2005 *Phys. Rev. B* **71** 014446

[30] Zhang J, Ye F, Sha H, Dai P, Fernandez-Baca J A and Plummer E W 2007 *J. Phys.: Condens. Matter* **19** 315204

[31] Louca D and Sarrao J L 2003 *Phys. Rev. Lett.* **91** 155501

[32] Hoch M J R, Kuhns P L, Moulton W G, Reyes A P, Wu J and Leighton C 2004 *Phys. Rev. B* **69** 014425

[33] Poienar M, Damay F, Martin C, Robert J and Petit S 2010 *Phys. Rev. B* **81** 104411

[34] Haraldsen J T, Ye F, Fishman R S, Fernandez-Baca J A, Yamaguchi Y, Kimura K and Kimura T 2010 *Phys. Rev. B* **82** 020404(R)

[35] Maier T A and Scalapino D J 2008 *Phys. Rev. B* **78** 020514(R)

[36] Ewings R A, Perring T G, Bewley R I, Guidi T, Pitcher M J, Parker D R, Clarke S J and Boothroyd A T 2008 *Phys. Rev. B* **78** 220501(R)

[37] Uemura Y J and Birgeneau R J 1986 *Phys. Rev. Lett.* **57** 1947
Uemura Y J and Birgeneau R J 1987 *Phys. Rev. B* **36** 7024

[38] Varma S and Tasdelen F More details on bi-orthogonality can be found in 2011 *Comput. Math. Appl.* **62** 3663

[39] Bouzerar G, Ziman T and Kudrnovský J 2005 *Europhys. Lett.* **69** 812

[40] Bouzerar G 2007 *Eur. Phys. Lett.* **79** 57007

[41] Chakraborty A and Bouzerar G 2010 *Phys. Rev. B* **81** 172406

[42] Chakraborty A, Bouzerar R and Bouzerar G 2011 *Eur. Phys. J. B* **81** 405

[43] Goennenwein S T B *et al* 2003 *Appl. Phys. Lett.* **82** 730

[44] Sperl M *et al* 2008 *Phys. Rev. B* **77** 125212

[45] Bergqvist L, Eriksson O, Kudrnovský J, Drchal V, Korzhavyi P and Turek I 2004 *Phys. Rev. Lett.* **93** 137202

[46] Sato K, Schweika W, Dederichs P H and Katayama-Yoshida H 2004 *Phys. Rev. B* **70** 201202(R)